



## Raman and infrared microscopic study on the lipid redistribution in Alzheimer diseased murine tissue

Alicia Schirer<sup>a</sup>, Youssef El Khoury<sup>a</sup>, Christine Patte-Mensah<sup>b</sup>, Christian Klein<sup>b</sup>,  
Laurence Meyer<sup>b</sup>, Monika Rataj-Baniowska<sup>b</sup>, David Moss<sup>c</sup>, Ayikoe-Guy Mensah-Nyagan<sup>b</sup>  
<sup>\*b</sup> Sophie Lecomte<sup>\*d</sup> and Petra Hellwig<sup>+a</sup>

<sup>a</sup>Laboratoire de bioélectrochimie et spectroscopie. UMR 7140, chimie de la matière complexe ; Université de Strasbourg-CNRS. ; 4, Rue Blaise Pascal 67081 Strasbourg, France.

<sup>b</sup>Biopathologie de la Myéline, Neuroprotection et Stratégies Thérapeutiques, INSERM U1119, Fédération de Médecine Translationnelle de Strasbourg (FMTS); Université de Strasbourg. 1 rue Eugène Boeckel, 67000 Strasbourg, France.

<sup>c</sup>Synchrotron Light Source ANKA, Karlsruhe Research Center, Karlsruhe, Germany, Hermann-von-Helmholtz-Platz 1, 76344 Eggenstein-Leopoldshafen, Germany.

<sup>d</sup>Chimie Biologie des Membranes et Nanoobjets, UMR 5248, Université de Bordeaux-CNRS. 14 Allée Geoffroy St. Hilaire, 33600 Pessac, France.

The Alzheimer disease (AD) is the most common form of dementia. Several stages characterize the neurodegenerative process from the early AD to severe AD. During these stages, major structural and molecular changes will spread throughout the cerebral cortex. Here, we present Raman and Infrared microscopic evidences for the reorganization of phospholipids in brain tissue from AD diseased tissues of mice with severe AD. On the basis of the imaging results, it can be shown that the lipid concentration around the aggregates increases and decreases in the plaques. In addition, a change of the ratio of unsaturated to saturated lipids is found pointing towards a changed metabolism. © Anita Publications. All rights reserved.

**Keywords:** Alzheimer disease; Raman microscopy, Infrared microscopy; Phospholipids; Aggregation Cascade .

### 1 Introduction

Alzheimer's disease (AD) is the most common neurodegenerative disorder and cause of dementia. The disease is identified pathologically by amyloid plaques composed of aggregated amyloid-peptide, neurofibrillary tangles composed of aggregated, hyperphosphorylated tau protein and neuron loss. Neurodegeneration in AD is a pathologic condition of cells rather than an accelerated way of aging. There is cumulative evidence from studies in cultured brain cells and on brains that oxidative stress constitutes a main factor in the modification of normal signaling pathways in neuronal cells, leading to biochemical and structural abnormalities and neurodegeneration as related to AD pathogenesis [1,2].

Most of the brain is composed of lipids, including sphingolipids, glycerophospholipids, and cholesterol [3-5]. In addition, the brain has a very high concentration of long-chain omega-3 and omega-6 fatty acids, even if the role of these fatty acids in the different signaling cascades and in AD is not understood [6-7].

---

Corresponding author

e mail: [hellwig@unistra.fr](mailto:hellwig@unistra.fr) (Petra Hellwig)

A crucial player in the AD cascade is the Amyloid precursor protein (APP) a type I transmembrane protein that is cleaved into amyloid  $\beta$ -peptide ( $A\beta$ ) by  $\beta$ - and  $\gamma$ -secretases [8-9]. APP is associated with lipid rafts, which are membrane domains enriched with cholesterol, sphingolipids, and gangliosides and that are essential for intracellular and vesicle transport [10-13]. Several studies suggest that both homeostasis of lipid composition and oxidation state of lipids, including DHA, are critical to APP processing even if these observations are still under debate [13-14].

It is well accepted that there is an age-related change in the lipid rafts composition and alterations in intracellular communication may be associated with age-associated reductions in synaptic plasticity. In neurodegenerative diseases, the composition of lipid rafts changes more rapidly [15]. Lipid raft aging appears to be enhanced in AD, which may be part of the process contributing to disrupted signal transduction, increased APP processing, and rapid formation of AB aggregates [16].

Raman and infrared microscopies are tools to monitor the distribution of molecules in biological tissues and thus the modification during the disease, but also the modification of the involved peptides and proteins [17-19]. These methods provided the possibility to examine also the localization of hemes [20] and lipids in the diseased tissues [21-23]. Here, we focus on murine samples of different ages. This is essential, since the monitoring of the effect of a treatment will be done in murine samples and it is necessary to demonstrate that the lipid redistribution in AD mice is similar to the human one.

## 2 Methods

### *Tissue preparation*

The procedures involving animals and their care were conducted in compliance with a European Communities Council Directive (86/609/EEC) and under the supervision of authorized investigators. The protocols were reviewed and approved by the Alsace Head Office of the French Department of Veterinary and Public Health Guide for the Care and Use of Laboratory Animals. We used female APPSWE hemizygote mice [B6, SJL-Tg (APPSWE) 2576 Kha, tested for heterozygous RD1, Taconic Europe, Denmark]. These Tg2576 mice, which carry a transgene coding for the 695-amino acid isoform of human Alzheimer  $\beta$ -amyloid precursor protein, are well characterized as developing  $A\beta$  plaques and progressive memory deficits with age, making them suitable for the investigation of the relationship between  $A\beta$  accumulation/degradation and cognitive performance [24-26]. We obtained the Tg2576 mice and their wild-type counterparts (WT) at the age of 6 months and after 4 weeks of adaptation to our local animal facilities, they were submitted to monthly behavioral analyses (from month 7 to 18) using the spatial novelty task to assess their cognitive performance. This task is based on the spontaneous tendency of mice to explore preferentially those objects which have been displaced within a familiar arrangement of objects. Tg 2576 mice are deeply impaired in this task, independently of the respiratory-deficient (rd) mutation [27,28]. After the behavioral characterization, 18-month-old Tg2576 mice (10) with severe cognitive deficit and WT mice (10) were killed, decapitated, and their brains were removed and rapidly frozen by immersion in isopentane (cooled at  $-40$  °C). Cryo-sections (10  $\mu$ m) of frozen mice brains were made with a Reichert-Jung, LEICA instrument and mounted on BaF<sub>2</sub> or CaF<sub>2</sub> windows for infrared and Raman measurements, respectively.

### *Infrared microspectroscopy*

Synchrotron FTIR microspectroscopy was performed at the beamline IR2 of the ANKA synchrotron facility (KIT, Karlsruhe, Germany) on an IRscope II infrared microscope (Bruker Optics, Germany) equipped with a 36 $\times$  objective. The infrared spectra were recorded in transmission mode with a spectral resolution of 4  $\text{cm}^{-1}$ , 128 co-added scans, 12.5  $\mu$ m aperture dimension and a step size of 4.16  $\mu$ m. The measuring range was 700-4500  $\text{cm}^{-1}$ . A background spectrum was collected from clean BaF<sub>2</sub> window after every 10 spectra.

### Raman microspectroscopy:

Raman microspectroscopy was performed on WITec Alpha300RS confocal Raman microscope using a frequency doubled Nd:YAG Laser at 532 nm. Raman spectra were recorded using a 20×/NA 0.4 in the 0-3800  $\text{cm}^{-1}$  range with an integration time of 0.05 s. A spectrum was recorded every 0.5  $\mu\text{m}$  along the x and y directions. The resolution was 2.9  $\text{cm}^{-1}$ .

### Spectral analysis

Infrared and Raman spectrochemical images were created with Cytospec v 2.00.01 and Witec softwares, respectively. For infrared measurements, plaques were characterized from the area of the  $\beta$ -sheet band at 1630  $\text{cm}^{-1}$ . Lipid distribution was based on the area of  $\text{CH}_2/\text{CH}_3$  bands between 3002-2829  $\text{cm}^{-1}$  and on the area of lipid carbonyl band between 1767-1724  $\text{cm}^{-1}$ . The level of unsaturated lipids was also investigated from the area under the curve between 3028-3002  $\text{cm}^{-1}$  ( $=\text{CH}$  vibration).

For Raman measurements, plaques were imaged from the intensity of the  $\beta$ -sheet band at 1670  $\text{cm}^{-1}$ . Lipid and proteins have characteristic vibrations between 3000 and 2800  $\text{cm}^{-1}$  ( $\nu\text{CH}_2/\text{CH}_3$ ) but lipids have a majority contribution between 2930 and 2800  $\text{cm}^{-1}$ . Thus, lipid distribution was studied from the area under the curve between 2936-2834  $\text{cm}^{-1}$  and the level of unsaturated lipids was examined from the area of the  $=\text{CH}$  band between 3031-3005  $\text{cm}^{-1}$ .

## 3 Results and Discussions

Figure 1 shows the direct comparison of the IR spectra obtained from healthy and diseased murine samples. The spectra of the healthy form display the characteristic infrared spectrum of a tissue and includes contributions from the carbonyl group of lipids at 1747  $\text{cm}^{-1}$  (as ester group of the phospholipids) and of the proteins and peptides that can be seen in the amide I and amide II modes, respectively (1662 and 1550  $\text{cm}^{-1}$ ). In the spectra of the diseased tissue the amide I is found shifted from 1662 to 1630  $\text{cm}^{-1}$ . The position of this signal is characteristic for the secondary structure and the shift is in line with the increase of peptides and proteins with a beta-type secondary structure and, thus, with the aggregation in the plaque, as previously described [29-33]. Interestingly the intensity of the signal at 1747  $\text{cm}^{-1}$  is decreasing in the spectra of the diseased tissue. This change can be attributed to a loss of lipids in the aggregates.

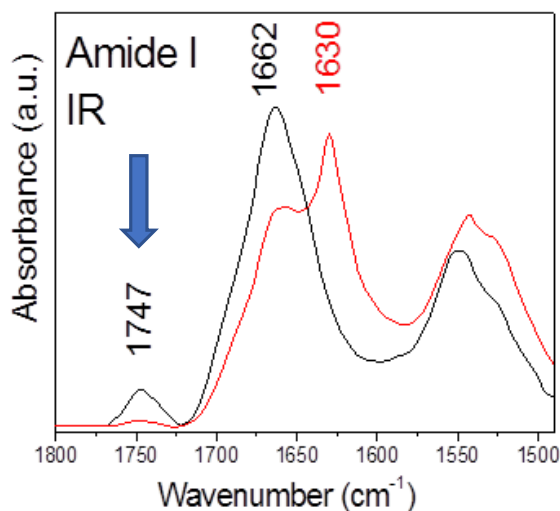
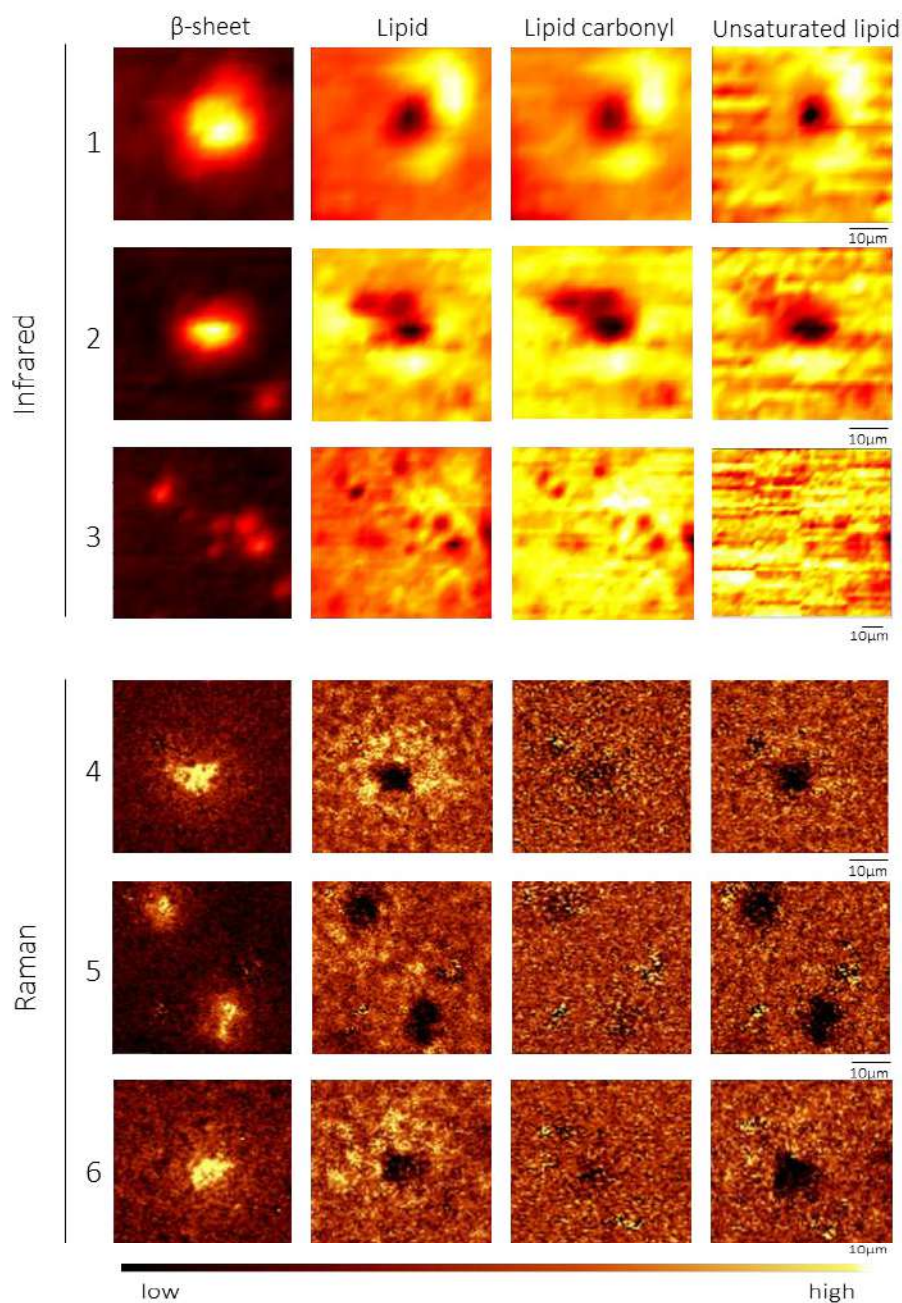


Fig 1. IR absorbance spectra of healthy (black line) and AD diseased sample (red line). The arrow highlights the increasing C=O signal for the lipids.



**Fig 2.** Infrared and Raman imaging of 6 different plaques from AD diseased murine tissues at the wavelengths characteristic for proteins in beta-sheet conformation and for lipids. Yellow corresponds to the highest intensity of specific marker bands (see details in the text), dark to the lowest.

In order to get further insight in the reorganization of these molecules, imaging was performed, both in infrared and Raman. Specific wavelengths are selected that correspond to selected functional groups, like the C=O mode of the lipid or of the backbone, as seen in Fig 1 above, or to the CH<sub>2</sub>/CH<sub>3</sub> modes

characteristic for saturated or unsaturated lipids. Figure 2 shows the infrared and the Raman imaging of 6 different examples of a plaque in diseased tissues. Imaging allows us visualizing the distribution of the lipids in the tissue. Yellow corresponds to the high signal intensity and black to a lower intensity. In all samples the concentration of proteins and peptides in a beta sheet secondary structure is significantly increased in the plaque, in line with previous reports [29-33].

When analyzing the intensity distribution of the different functional groups the observation made in Fig 1 is confirmed: the intensity of the signals associated with the formation of beta sheet peptides aggregates increases and the lipid content decreases in the plaques 1, 2, 4-6, only in the example Nr 3, the lipid reorganization is less clear and also the aggregate is less well formed. The imaging approach allows us to reveal that the lipids are cumulating around the aggregates, and this is seen from both techniques Raman and Infrared microscopy. The Raman images obtained for samples 4-6 indicate; that the lack of lipids in the plaque predominantly, but not exclusively concerns unsaturated lipids. It cannot be determined from the data if both processes are taking place at the same time, or if the lipids are accumulated around the plaque to protect the cell. In an alternative explanation, the interaction of the aggregating peptides with the lipid will induce the accumulation of the lipids rafts themselves.

Importantly, the observations made here can be correlated with data previously presented for human samples [20]. It is noted that we cannot provide evidence on when this reorganization takes place, even if it seems to be happening in a corroborated manner. In spectra from murine samples at an earlier stage of the disease when no plaque is observed, no redistribution of the lipids is seen at the given resolution of about 1 micrometer. The reorganization of the lipids is thus an intrinsic property of the late AD diseased tissue.

In conclusion, Raman and IR microscopic data allowed visualizing the reorganization of the lipids in the tissues in AD diseased tissue. This observation is crucial for the understanding of the different processes that take place during the aggregation cascade.

## References

1. LaFerla F M, Oddo S, Alzheimer's disease: A $\beta$ , tau and synaptic dysfunction. *Trends Mol Med*, 11(2005)170–176.
2. Zhao Y, Zhao B, Oxidative stress and the pathogenesis of Alzheimer's disease. *Oxid. Med. Cell. Longev*, 2013(2013) 316523; /doi.org/10.1155/2013/316523.
3. Svennerholm L, Bostrom K, Jungbjer B, Olsson L, Membrane lipids of adult human brain: lipid composition of frontal and temporal lobe in subjects of age 20 to 100 years, *J Neurochem*, 63(1994)1802–1811.
4. O'Brien J S, Sampson E L, Lipid composition of the normal human brain: gray matter, white matter, and myelin. *J Lipid Res*, 6(1965)537–544.
5. Kishimoto Y, Agranoff B W, Radin N, Burton R M, Comparison of the fatty acids of lipids of subcellular brain fractions, *J Neurochem*, 16(1969)397–404.
6. Torres M, Price S L, Fiol-Deroque M A, Marcilla-Etxenike A, Ahyayauch H, Barcelo-Coblijn G, Terés S, Katsouri L, Ordinas M, López D J, Iburguren M, Goñi F M, Busquets X, Vitorica J, Sastre M, Escribá P V, Membrane lipid modifications and therapeutic effects mediated by hydroxydocosahexaenoic acid on Alzheimer's disease, *Biochim Biophys Acta*, 1838(2014)1680–1692.
7. Mohaibes R J, Fiol-deRoque M A, Torres M, Ordinas M, Lopez D J, Castro J A, Escribá P V, Busquets X, The hydroxylated form of docosahexaenoic acid (DHAH) modifies the brain lipid composition in a model of Alzheimer's disease, improving behavioral motor function and survival, *Biochim Biophys Acta Biomembr*, 1859(2017)1596–1603.
8. Nunan J, Small D H, Regulation of APP cleavage by alpha-, beta- and gamma-secretases, *FEBS Lett*, 483(2000) 6–10.
9. Hartmann D, A brief history of APP secretases, their substrates and their functions, *Curr Alzheimer Res*, 9 (2012) 138–139.
10. Ehehalt R, Keller P, Haass C, Thiele C, Simons K, Amyloidogenic processing of the Alzheimer beta-amyloid precursor protein depends on lipid rafts, *J Cell Biol*, 160(2003)113–123.
11. Yoon I S, Chen E, Busse T, Repetto E, Lakshmana M K, Koo E H, Kang D E. Low-density lipoprotein receptor-related protein promotes amyloid precursor protein trafficking to lipid rafts in the endocytic pathway, *FASEB J*, 21(2007)2742–2752.

12. Marquer C, Devauges V, Cossec J C, Liot G, Lecart S, Saudou F, Duyckaerts C, Leveque-Fort S, Potier M C Local cholesterol increase triggers amyloid precursor protein-Bace1 clustering in lipid rafts and rapid endocytosis, *FASEB J*, 25(2011)1295–1305.
13. Bhattacharyya R, Barren C, Kovacs D M Palmitoylation of amyloid precursor protein regulates amyloidogenic processing in lipid rafts, *J Neurosci*, 33(2013)11169–11183.
14. Grimm M O, Rothhaar T L, Grosgen S, Burg V K, Hundsdoerfer B, Hauptenthal V J, Friess P, Kins S, Grimm H S, Hartmann T, Trans fatty acids enhance amyloidogenic processing of the Alzheimer amyloid precursor protein (APP), *J Nutr Biochem*, 23(2012)1214–1223.
15. Li M Z, Zheng L J, Shen J, Li X Y, Zhang Q, Bai X, Wang Q S, Ji J G. SIRT1 facilitates amyloid beta peptide degradation by upregulating lysosome number in primary astrocytes, *Neural Regen Res*, 13(2018)2005–2013.
16. Grassi S, Giussani P, Mauri L, Prioni S, Sonnino S, Prinetti A, Lipid rafts and neurodegeneration: structural and functional roles in physiologic aging and neurodegenerative diseases, *J Lipid Res*, 61(2019)636–654.
17. Kretlow A, Wang Q, Kneipp J, Lasch P, Beekes M, Miller L, Naumann D, FTIR-microspectroscopy of prion-infected nervous tissue, *Biochim Biophys Acta*, 1758(2006)948–959.
18. Miller L M, Dumas P, Chemical imaging of biological tissue with synchrotron infrared light, *Biochim Biophys Acta*, 1758(2006)846–857.
19. Ooi G J, Fox J, Siu K, Lewis R, Bamberg K R, McNaughton D, Wood B R, Fourier transform infrared imaging and small angle x-ray scattering as a combined biomolecular approach to diagnosis of breast cancer, *Med Phys*, 35(2008)2151–2161.
20. El Khoury Y, Schirer A, Patte-Mensah C, Klein C, Meyer L, Rataj-Baniowska M, Bernad S, Moss D, Lecomte S, Mensah-Nyagan A G, Hellwig P, Raman Imaging Reveals Accumulation of Hemoproteins in Plaques from Alzheimer's Diseased Tissues, *ACS Chem Neurosci*, 12(2021)2940–2945.
21. Benseny-Cases N, Klementieva O, Cotte M, Ferrer I, Cladera J. Microspectroscopy ( $\mu$ FTIR) reveals co-localization of lipid oxidation and amyloid plaques in human Alzheimer disease brains. *Anal Chem*, 86 (2014)12047–12054.
22. Liao C R, Rak M, Lund J, Unger M, Platt E, Albensi B C, Hirschmugl C J, Gough K M, Synchrotron FTIR reveals lipid around and within amyloid plaques in transgenic mice and Alzheimer's disease brain, *Analyst*, 138(2013)3991–3997.
23. Kiskis J, Fink H, Nyberg L, Thyr J, Li J Y, Enejder A, Plaque-associated lipids in Alzheimer's diseased brain tissue visualized by nonlinear microscopy, *Sci Rep*, 5(2015)13489; doi.org/10.1038/srep13489.
24. Hsiao K, Chapman S, Nilsen P, Eckman C, Harigaya Y, Younkin S, Yang F, Cole G, Correlative memory deficits, A $\beta$  elevation, and amyloid plaques in transgenic mice, *Science*, 274(1996)99–102.
25. Westerman M A, Cooper-Blacketer D, Mariash A, Kotilinek L, Kawarabayashi T, Younkin L H, Carlson G A, Younkin S G, Ashe K H, The Relationship between A $\beta$  and Memory in the Tg2576 Mouse Model of Alzheimer's Disease, *J Neurosci*, 22(2002)1858–1867.
26. Mawuenyega K G, Sigurdson W, Ovod V, Munsell L, Kasten T, Morris J C, Yarasheski K E, Bateman R J, Decreased clearance of CNS  $\beta$ -amyloid in Alzheimer's disease, *Science*, 330(2010)1774; doi.10.1126/science.1197623.
27. Ognibene E, Middei S, Daniele S, Adriani W, Ghirardi O, Caprioli A, Laviola G, APP transgenic mice for modelling behavioral and psychological symptoms of dementia (BPSD), *Behav Brain Res*, 156(2005)225–232.
28. Yassine N, Lazaris A, Dorner-Ciossek C, Despres O, Meyer L, Maitre M, Mensah-Nyagan A G, Cassel J C, Mathis C, Detecting spatial memory deficits beyond blindness in tg2576 Alzheimer mice, *Neurobiol Aging*, 34(2013)716–730.
29. Barth A, Infrared spectroscopy of proteins, *Biochim Biophys Acta*, 1767(2007)1073–1101.
30. Krimm S, Bandekar J, Vibrational spectroscopy and conformation of peptides, polypeptides, and proteins, *Adv Protein Chem*, 38(1986)181–364.
31. Chirgadze Y N, Nevskaya N A, Infrared spectra and resonance interaction of amide-I vibration of the antiparallel-chain pleated sheet, *Biopolymers*, 15(1976)607–625.
32. Qiang W, Yau W M, Luo Y, Mattson M P, Tycko R, Structural Variation in Amyloid- $\beta$  Fibrils from Alzheimer's Disease Clinical Subtypes, *Proc Natl Acad Sci (U S A)*, 109(2012) 4443–4448.
33. Berthelot K, Ta H P, Gean J, Lecomte S, Cullin C, *In vivo* and *in vitro* analyses of toxic mutants of HET-s: FTIR antiparallel signature correlates with amyloid toxicity, *J Mol Biol*, 412(2011)137–152.

[Received: 10.01.2022; revised recd: 12.01.2022; accepted: 13.01.2022]